Explosions throughout the universe

Neil Gehrels

Astroparticle Physics Division,
NASA/Goddard Space Flight Center,
Greenbelt, MD 20771, USA
neil.gehrels@nasa.gov

John K. Cannizzo

CRESST/Joint Center for Astrophysics,
University of Maryland, Baltimore County,
Baltimore, MD 21250, USA
john.k.cannizzo@nasa.gov

High energy transients make up a diverse and exotic class of objects, from terrestrial lightning to γ-ray bursts at cosmological distances. In this review, we provide a detailed look at some of the more exciting transients observed over the last few years by *Swift* and other high energy missions.

Keywords: Black hole physics; radiation mechanisms; nonthermal; stars; activity; gamma-ray burst; general; stars; neutron; novae; galaxies; star formation.

1. *Swift* – A Time Domain Observatory

The *Swift* mission[1] was built by an international team from the US, UK and Italy. After five years of development it was launched from Kennedy Space Center on 20 November 2004. Full normal operations commenced on 5 April 2005.

Swift carries three scientific instruments:

BAT (15–300 keV). The burst alert telescope[2] utilizes a coded-aperture mask of 52,000 randomly placed 5 mm Pb tiles 1 m from a detector plane consisting of 32,768 four mm CdZnTe detector tiles. The shadow cast by a γ-ray source onto the detector plane by the Pb tiles allows for a $\sim$1–4 arcmin source sky localization within 15 s, which is promptly relayed to ground robotic instruments. BAT has a large field-of-view (FOV) — $\sim$1 sr fully coded, and $\sim$3 sr partially coded.

XRT (0.3–10 keV). The X-ray telescope[3] is a Wolter 1 grazing incidence, imaging XRT with a 120 cm^2 effective area (1.5 keV), 23.6 arcmin $\times$ 23.6 arcmin FOV, point spread function (PSF) half-power diameter of 18 arcsec (7 arcsec FWHM), and sensitivity of $\sim 2 \times 10^{-14}\,\mathrm{erg\,cm^{-2}\,s^{-1}}$ in 10^4 s.

UVOT (170–650 nm). The UV-optical telescope[4] is a modified Ritchey–Chrétien reflector with 30 cm aperture, 17 arcmin $\times$ 17 arcmin FOV, 1.9 arcsec FWHM PSF (350 nm), and limiting magnitude 23 in white light in 10^3 s.

Swift catches about two GRBs in a week, and carries out about three ToO observations a day.

2. A Potpourri of High Energy Transients

Table 1 indicates the wide range of classes of high energy transients, along with their associated energies. In this section, we preview the topic by examining two completely different classes of high energy transients, one terrestrial (γ-ray flashes) (TGFs) and one galactic (soft gamma repeaters).

Terrestrial γ-ray flashes were first seen by the burst and transient source experiment (BATSE) on the *compton gamma-ray observatory*. They are thought to be due to decaying electric fields above thunderclouds after a lightning discharge. Relativistic electrons interact with nuclei of atoms in the atmosphere and produce γ-rays via bremsstrahlung. A process known as runaway electron avalanche is thought to be relevant, but the details are uncertain.[5,6] Subsequent observations by the *Reuven Ramaty high energy solar spectroscopic imager* (RHESSI) have revealed TGFs with much higher energies, and show that $\sim$500 TGFs occur per day, which is a small fraction of the total number of daily lightning strikes on Earth (~ 3–4×10^6). This estimate excludes effects relating to beaming and atmospheric obscuration of low altitude TGFs. The *Fermi*/GBM is currently detecting TGFs at a rate of $\sim 100\ \mathrm{yr}^{-1}$; some are even detected by *Fermi*/LAT during special Earth-pointed observations. This high rate has held since 2009 when the BGOs were included in the triggering algorithm. Perhaps the most spectacular discovery has been that of 511 keV emission from e^+/e^- annihilation in TGFs.[7] It is unsettling to consider the fact that terrestrial processes are capable of producing antimatter in significant quantities.

Soft gamma repeaters (SGRs) emit bursts of γ-rays and X-rays which are thought to be due to the rearrangement of powerful magnetic fields in magnetars — pulsars with magnetic fields of $\sim 10^{15}$ G. The first one seen was the "March 5th Event" from 1979 which was observed by two Soviet interplanetary spacecraft *Venera* 11 and *Venera* 12.[8] This event, SGR 0526-66, was localized to the SN remnant N49 in the LMC. Given a distance of $\sim$50 kpc, the isotropic equivalent energy emitted was $\sim 5 \times 10^{44}$ erg, compared to $\sim 10^{41}$ erg for a typical SGR burst. A $\sim$8 s periodicity thought to be the NS spin period is plainly evident in the data. Thompson and Duncan[9] present an extensive model of the March 5th event and other SGRs as magnetars, i.e. $B \simeq 10^{15}$ G. They argue that the March 5 burst was due

Table 1. X-ray/γ-ray transients.

Source	Energy source	E(γ-ray)
Lightning	E field	10^{10} erg
γ-ray burst	Gravity	10^{52} erg
Magnetar	B field	10^{44} erg
Tidal disruption	Gravity	10^{52} erg
Stellar flare	B field	10^{32} erg
Supernova/nova	Nuclear	10^{49} erg
Accreting BH/NS	Gravity	$10^{36}\ \mathrm{erg\,s^{-1}}$
AGN	Gravity	$10^{43}\ \mathrm{erg\,s^{-1}}$

to a large-scale readjustment of the stellar magnetic field, while the more standard SGR bursts are caused by the release of magnetic stresses within a more localized patch of the crust. Thompson and Duncan put forth a variety of independent arguments in favor of the magnetar scenario, including (i) the necessity of a very high B-field to spin down the pulsar to $\sim$8 s within the inferred $\sim 10^4$ yr age of N49, (ii) a very strong B-field suppresses the e^--scattering cross section below the standard Thomson value by the ratio $\sim (B/B_{\rm QED})^{-2}$, where $B_{\rm QED} = m_e^2 c^2/(e\hbar) = 4.4\times 10^{13}$ G (the point at which the nonrelativistic Landau energy $\hbar eB/(m_e c)$ equals the electron rest energy $m_e c^2$), therefore enabling $L \simeq 10^4 L_{\rm Edd}$ for surface fields $\gtrsim 10^{14.5}$ G, (iii) persistent X-ray emission from SGR 0526-66 at $\simeq 7 \times 10^{35}$ erg s^{-1}[10,11] implies $B_{\rm crust} \gtrsim 10^{15}$ G, and (iv) an identification of the $\sim$0.15 s duration of the hard spike of the March 5 event[8,12] with the internal Alfvén crossing time leads to $B \simeq 7 \times 10^{14}$ G.

On August 27, 1998 a second giant flare from an SGR was seen. SGR 1900+14 became the brightest extra-solar system γ-ray source ever. The 5.16 s spin period of the pulsar could be easily seen directly in the light curve.[13] The flare was so bright that it produced 5.16 s ionization modulations in the upper atmosphere of the Earth. Thompson and Duncan[14] argue that the extremely high luminosity $L \gtrsim 10^6 L_{\rm Edd}$ during the initial $\sim$0.5 s spike in SGR 1900+14 demands $B \gtrsim 10^{15}$ G. Shortly after the launch of *Swift*, on 27 December 2004, a giant γ-ray flare was seen from SGR 1806-20 with a peak flux of $\sim$5 erg cm^{-2} s^{-1}. SGR bursts are much brighter than ordinary X-ray bursts, which are due to thermonuclear flashes of accumulated hydrogen on the surface of a NS ($L \sim 10^3$–$10^4 L_{\rm Edd}$ versus. $L \sim L_{\rm Edd}$), and they also have harder spectra than ordinary X-ray bursts.

3. DG CVn Superflare

A basic fact of stellar structure is that early spectral type stars O-B-A have convective cores and radiative envelopes, whereas later spectral type stars A-F-G-K-M have radiative cores and convective envelopes. The dividing point lies at two solar masses which corresponds roughly to an A4 star. Our G2 sun is convective over its outermost 30% in radius. Late type M stars are completely convective ($\lesssim 0.4 M_\odot$). In a subset of stars of late spectral type the combination of surface convection and high rotation can lead to strong expulsion of magnetic fields from the stellar surface. In stars with outer convection a dynamo operates at the base of the convective envelope, twisting internal dipole field into a tangled geometry. Magnetic buoyancy expels field from the photosphere as active regions. Loops arch outward from the stellar surface, extending from "−" to "+" polarity. Where two loops cross, one can have a massive reconnection event — a superflare.

By contrast, although early spectral type stars such as Ap and Am can have strong magnetic fields, they are convective only at their cores and therefore do not actively transport B-field to outside the star. Thus, they do not have stellar flares. Their high fields are only evidenced through Zeeman splitting of photospheric spectral lines.

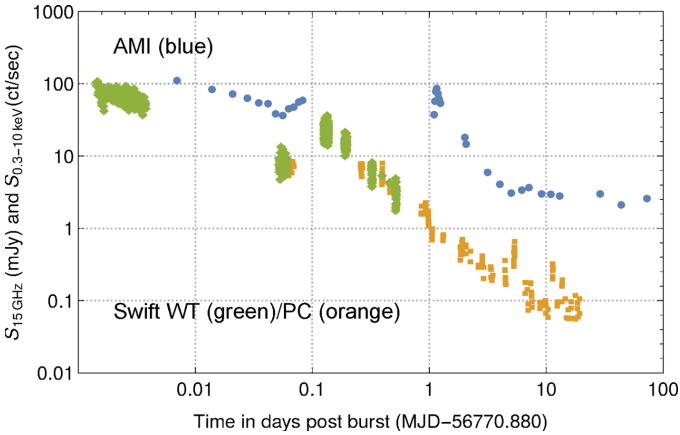

Fig. 1. (Color online) Superflare from the DG Cvn.[16] Light curves are from AMI-LA 13–18 GHz (blue circles) and *Swift*/XRT WT/PC (green diamonds/orange squares) 0.3–10 keV. In X-rays, the source was brightest at the first measurement, $T0+2$ min and then declined for $\sim$1 h, rebrightening at $0.075 < (t - T0) < 0.125\,d$. The radio flux behaved similarly, with a strong detection in the first measurement at $T0 + 6$ min followed by a decline and subsequent rebrightening. A second radio flare occurred at $\sim T0 + 1.1\,d$.

DG CVn, a close visual dM4e+dM4e binary with orbital separation $\sim$3 AU, is a known flare star system. Both stars have masses and radii $\sim$1/3 solar. At 18 pc the system is relatively close. Its kinematics identify it as being young, $\sim$30 Myr, and furthermore at least one of the stars is a fast rotator with $v \sin i \simeq 50\,\mathrm{km\ s^{-1}}$. For comparison, if our sun were examined spectroscopically from several pc at a random orientation it would have $v \sin i \approx 1$–$2\,\mathrm{km\,s^{-1}}$.

On 23 April 2014 *Swift*/BAT detected a superflare in DG CVn which reached 0.3 Crab in the 15–150 keV BAT band. The flare arose from one of the stars in the binary. It consisted of a series of outbursts; the strongest was $\sim 10^4$ times more energetic than the largest solar flare ever seen — the Carrington Event of 1859. Time resolved spectral fitting at the peak of the flare implies $T \simeq 2 \times 10^8$ K and $L_X \simeq 1.9 \times 10^{32}$ erg s^{-1} within the XRT 0.3–10 keV window. This compares with a normal systemic bolometric luminosity 1.3×10^{32} erg s^{-1}. As with a previous superflare seen in 2008 in EV Lac,[15] for several minutes the X-ray emission from the flare outshone the total light from the system.

Alerted by the *Swift*/BAT trigger, Fender *et al.*[16] detected a bright ($\sim$100 mJy) radio flare using AMI-LA (Fig. 1, from Ref. 16). This is the earliest detection ever made of bright, prompt, radio emission from a high-energy transient. Although radio emission is known to be associated with active stars, this was the first detection of a large radio flare in conjunction with a gamma-ray superflare.

4. RS Oph Nova

Classical and recurrent novae happen in interacting binaries containing a white dwarf (WD) accretor and are due to the thermonuclear detonation of accreted

material on the surface of a WD.[17] This can occur if the temperature and pressure at the base of the accumulated layer of accreted matter are in the appropriate regime. *Swift* has opened a new window on nova studies. An overview of the *Swift* sample of novae (52 galactic plus Magellanic Cloud) is given by Schwarz *et al.*[18] *Swift* has detected keV emission from shocked ejecta and supersoft (SS) emission from the WD surface.

RS Oph is a recurrent nova consisting of a red giant (RG) donor and a WD accretor residing in a semi-detached (i.e. mass-exchange) binary. About every 20 yr enough material from the RG accumulates on the surface of the WD to produce a thermonuclear explosion. On 12 February 2006 a new eruption occurred, reaching $m_V \simeq 4.5$. Detailed analysis of *Swift* observations (Fig. 2, from Ref. 19) indicated a mass ejection of $\sim 3 \times 10^{-5} M_\odot$ at $\sim$4,000 km s^{-1} into the wind of the mass losing RG companion in the system.[19]

Supersoft sources (SSSs) are powered by residual nuclear burning on the WD surface following the main nova eruption. Once the nova shell has expanded sufficiently it can become optically thin to 0.2–1 keV X-rays so that we can see all the way down to the WD surface and directly observe the nuclear reactions.

RS Oph is unusual in at least three respects compared to most novae: (i) The WD in the system is fairly massive so that the residual nuclear burning happens at a relatively high temperature, $T_{\rm eff} \simeq 10^6$ K, and the resultant emission fills the 0.3–1 keV bandpass. (ii) Its distance is only $\sim$2.5–3 kpc which makes it bright. (iii) RS Oph has a wide orbit with a RG donor instead of a red dwarf. Thus, it is an "embedded nova" because the shell runs into gas previously ejected in the RG wind. Therefore, embedded novae are brighter in hard X-rays $\sim 10^{36}$ erg s^{-1} than normal novae.

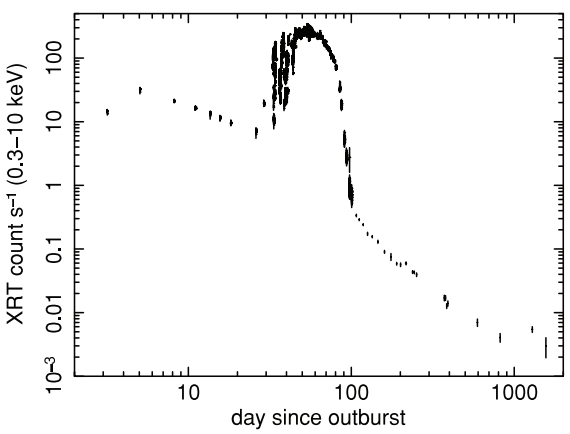

Fig. 2. Entire 0.3–10 keV *Swift*/XRT light curve of the 2006 outburst of the recurrent nova RS Oph.[19] The supersoft phase is prominent between days 29 and 100.

Could it be that SSS novae represent transitional objects between normal novae and Type Ia (single degenerate supernovae)? Not likely. It appears that all novae have the potential to be detected as SSS, and we have plenty examples of SSS, all novae, within several kpc. However, selection effects can prevent detection, especially if the absorbing column is too great. We can see the SSS inside a nova if the absorbing column $N_H \lesssim 2 \times 10^{21}\,\mathrm{cm}^{-2}$.[19]

5. V404 Cygni — Currently in Outburst

The microquasar V404 Cyg (also designated GS 2023+338) is a low-mass X-ray binary (LMXB) with a 6.5 d orbital period and a mass function $f = 6.3 M_\odot$.[20] Combining the mass function with spectroscopic data yields a central black hole mass of $\sim 12 M_\odot$. Radio parallax yields a distance 2.39 ± 0.14 kpc.[21] Its unusually hard and bright quiescent spectrum may indicate the presence of an advection dominated accretion flow, or ADAF.[22] V404 Cyg displays infrequent outbursting behavior, thought to be due to the accretion disk limit cycle mechanism, wherein long periods of inactivity correspond to times of mass accretion within the accretion disk, followed by brief periods of activity during which some fraction of the stored mass is accreted onto the central BH.[23–25] Due to a combination of larger dimensions (i.e. wider binaries) plus lower secondary mass transfer rates, the quiescent intervals for LMXBs can span decades, in contrast to weeks or months for cataclysmic variables, which undergo the same type of storage limit cycle accretion disk instability.[26] Also, a few LMXBs, such as A0620-00, exhibit smooth FRED-type outbursts (fast rise-exponential decay), whereas others, such as V404 Cyg, show chaotic outbursting behavior, perhaps indicating jetted emission. During the course of its outburst cycle, an LMXB traverses a familiar "turtle diagram" in hardness ratio versus flux, cycling through various combinations of high-low and hard-soft states.[27,28]

After 25 years of quiescence, V404 Cyg became active in 2015 June.[29] Historically, it was known to exhibit extremely bright and variable outbursts in all wavelengths. It is a prime candidate for exploring the connection between accretion and ejection, which require simultaneous observations at several wavelengths. Rodriguez *et al.*[29] present the results of long, nearly uninterrupted *INTEGRAL* observations and obtain light curves from the optical through soft γ-rays (Fig. 3, from Ref. 29). V404 Cyg was extremely variable in all wavebands, exhibiting 18 flares exceeding 6 Crab (20–40 keV) in $<3\,d$. Some of the optical flares occurred in conjunction with the X-ray flares, while others were delayed $\gtrsim$10 min. Rodriguez *et al.*[29] suggest that the first kind were associated with X-ray reprocessing by an accretion disk or the companion star, while the latter were due to plasma ejections, also seen in the radio. King *et al.*[30] analyze two *Chandra* exposures of V404 Cyg. They propose that strong P-Cygni profiles seen in high flux states are due to winds associated with the disruption of the outer accretion disk by radiation pressure as the luminosity approaches Eddington.

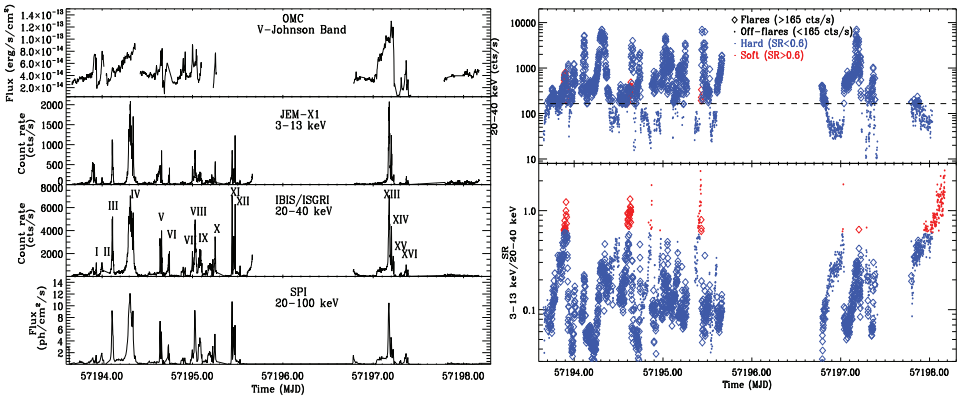

Fig. 3. *INTEGRAL* light curves of the 2015 outburst of V404 Cyg.[29] The left panel shows light curves in four different wave bands, and the right panel gives the 20–40 keV count rate (top) and f(3–13 keV)/f(20–40 keV) softness ratio (bottom). The dashed horizontal line indicates 1 Crab (20–40 keV). MJD 57193 corresponds to 2015 June 20.

6. SN 2008D Shock Breakout

The $t = 0$ time of a SN is marked by a burst of neutrinos, thus the "delayed" optical light from radioactivity in the ejecta through which most SNe are discovered does not provide information about the first moments following the explosion. On 9 January 2008 *Swift*/XRT serendipitously discovered an extremely bright X-ray transient (Fig. 4, from Ref. 31) while carrying out a preplanned observation of the nearby ($d = 27$ Mpc) galaxy NGC 2770.[31] Two days earlier XRT had observed the same location and did not see a source. X-ray outburst (XRO) 080109 lasted about 400 s and occurred in one of the galaxy's spiral arms. XRO 080109 was not a GRB (no γ-rays were detected), and the total X-ray energy $E_x \simeq 2 \times 10^{46}$ erg was orders of magnitude lower than a GRB. The peak luminosity $\sim 6 \times 10^{43}$ erg s^{-1} is much greater than the Eddington luminosity for a $\sim 1 M_\odot$ object, and also from Type I X-ray bursts. Therefore, the standard accretion and thermonuclear ash scenarios are excluded.

Simultaneous *Swift*/UVOT observations did not reveal a counterpart, but UVOT observations at 1.4 h showed a brightening. Gemini-North observations beginning at 1.7 *d* revealed a spectrum suggestive of a young SN.[31] Later observations confirmed the spectral features. The transient was classified as a Type Ibc SN based on the lack of H, and weak Si features.

Soderberg *et al.*[31] argue that the X-ray flash (XRF) indicates a trans-relativistic shock breakout from a SN, where the radius at breakout is $> 7 \times 10^{11}$ cm, and the shock velocity at breakout $\beta\gamma \lesssim 1.1$. They estimate a circumstellar density which yields an inferred pre-SN mass loss rate $\sim 10^{-5} M_\odot\,\mathrm{yr}^{-1}$, reinforcing the notion of a Wolf–Rayet progenitor. The similarity between the shock break-out properties of the He-rich SN 2008D and the He-poor GRB-associated SN 2006aj are consistent with a dense stellar wind around a compact Wolf–Rayet progenitor.

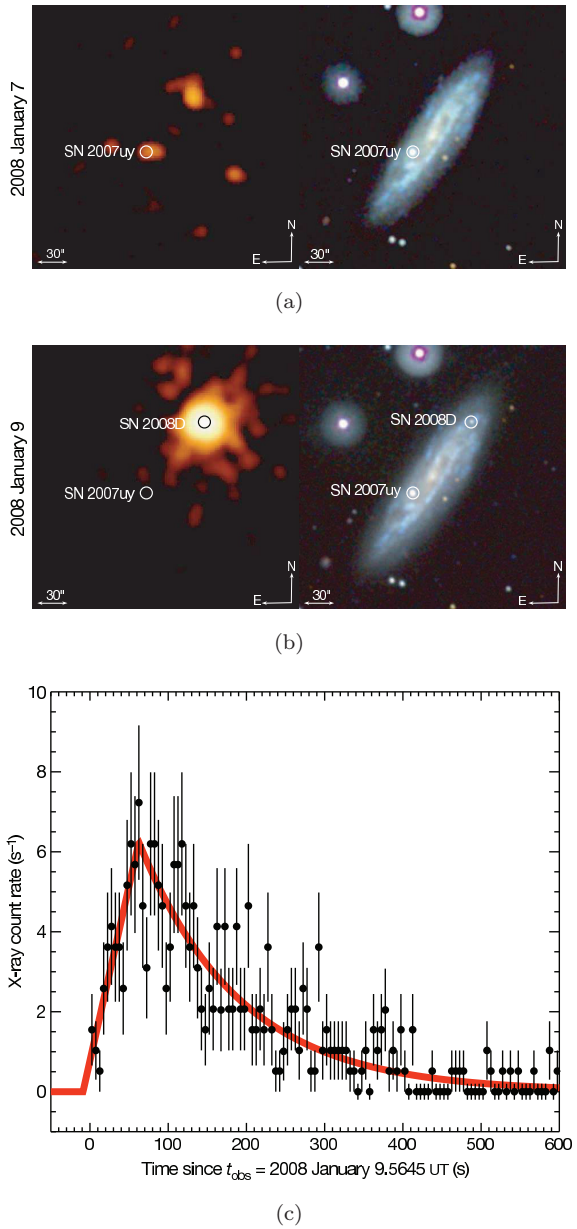

Fig. 4. X-ray (panels a,b–left) and optical (panels a,b–right) discovery images for SN2008D.[31] Panel c shows the *Swift*/XRT X-ray light curve.

Mazzali *et al.*[32] highlight several unusual features associated with SN 2008D/XRF 080109: (i) a weak XRF, (ii) an early, narrow optical peak, (iii) the disappearance of the broad lines characteristic of SN Ic HNe, and (iv) the development of He lines as in SNe Ib. By analyzing its light curve Mazzali *et al.*[32] infer a

SN energy $\sim 6 \times 10^{51}$ erg and ejected mass $\sim 7 M_\odot$, placing it between normal SNe Ibc and HNe. Mazzali *et al.*[32] conclude that SN 2008D was among the weakest explosions producing relativistic jets, in accordance with the inference of Soderberg *et al.*[31] of a trans-relativistic shock breakout.

7. Sgr A* Flares

The closest and best studied SMBH lies at the heart of our galaxy, in Sgr A*. Its bolometric luminosity is lower than expected from an Eddington-limited SMBH of mass $\sim 4 \times 10^6 M_\odot$ by a factor $\sim 10^8$–10^9, indicating the heyday of its quasarlike youth is well past. It has long since depleted its "loss cone"[33,34] supply of stars and gas and its very low accretion rate is generally characterized by a radiatively inefficient accretion flow.[35–38] Sgr A* emits a steady luminosity $\sim 2 \times 10^{33}$ erg s^{-1} in the soft X-ray band,[39] with occasional flaring up by a factor $\sim$5–150 for tens of minutes to hours. For $\sim$5 yr beginning in 2006, *Swift*/XRT observed a $\sim 21' \times 21'$ region around Sgr A*. Six flares were seen, with luminosities $\sim$(1–3)$\times 10^{35}$ erg s^{-1} (Fig. 5, from Ref. 40). Based on the number of observed flares and the total length of observations, Degenaar *et al.*[40] estimate a flaring rate 0.1–0.2 d^{-1}. This implies a bright flare with $L_X \simeq 10^{35}\,\mathrm{erg\,s^{-1}}$ occurs every $\sim$5–10 d. This rate is in accord with previous estimates based on *Chandra* data.[39]

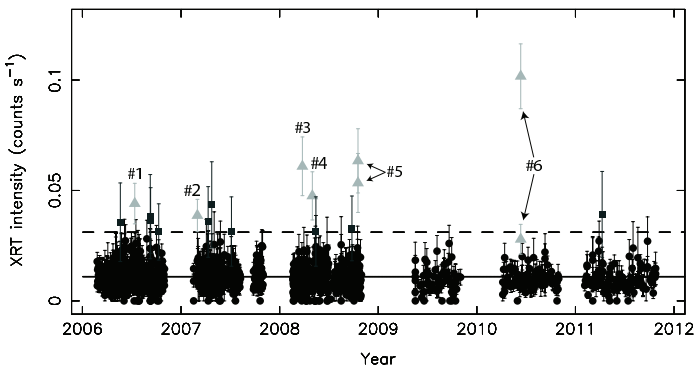

Fig. 5. Long term 0.3–10 keV *Swift*/XRT light curve of Sgr A*.[40] Solid horizontal line indicates the mean count rate observed in 2006–2011, whereas the dashed line indicates the 3σ level. The six confirmed X-ray flares are numbered and indicated by light gray triangles.

8. Swift J1644+57 — The First Jetted Tidal Disruption Event

Tidal disruption events (TDEs) are caused by the tidal disruption of stars that venture too close to the massive black holes (MBHs) at the centers of galaxies.[41–43] Prior to March 2011, nearly all our observational information was based on optical/UV studies[44,45] or long-term X-ray data with poor time sampling.[46] This

changed with the discovery by *Swift* of GRB 110328A/Swift J1644+57, a TDE viewed down the jet axis of a MBH in the nucleus of a galaxy at $z = 0.354$.[47–50]

A TDE occurs when the radius of closest approach R_P of a star passes within the tidal disruption radius R_T. After a TDE occurs, there is no accretion of shredded stellar material onto the SMBH for a time $\sim t_{\rm fb}$, the fallback time for the most tightly bound debris. Therefore, one expects a gap of $\sim t_{\rm fb}$, after which accretion can begin. In addition, Tchekhovskoy *et al.*[51] point out there will also be an additional $\Delta t_{\rm offset}$ after accretion starts before the jet activates. Thus, one anticipates a total time interval $t_{\rm int} \equiv t_{\rm fb} + \Delta t_{\rm offset}$ between TDE and an observed jet activity, i.e. flaring followed by a decay $\propto (t/t_{\rm int})^{\alpha}$. Thus, in an idealization in which (i) we view the TDE down the jet axis, (ii) the jet power tracks the rate of accretion onto the SMBH, and (iii) most of the jet power comes out in X-rays,

$$f_X = \begin{cases} 0 & t < t_{\rm int} \\ f_X, \max\left(\dfrac{t}{t_{\rm int}}\right)^{\alpha} & t \geq t_{\rm int}. \end{cases} \quad (1)$$

By considering the ratio of the peak X-ray flux to the fluence $\Delta E_X = \int_{t_{\rm int}}^{\infty} f_X(t)dt$, one can directly measure $t_{\rm fb} + \Delta t_{\rm offset}$. From the functional form for $f_X(t)$ one may write

$$t_{\rm fb} + \Delta t_{\rm offset} = -(1+\alpha)\frac{\Delta E_X}{f_X, \max}. \quad (2)$$

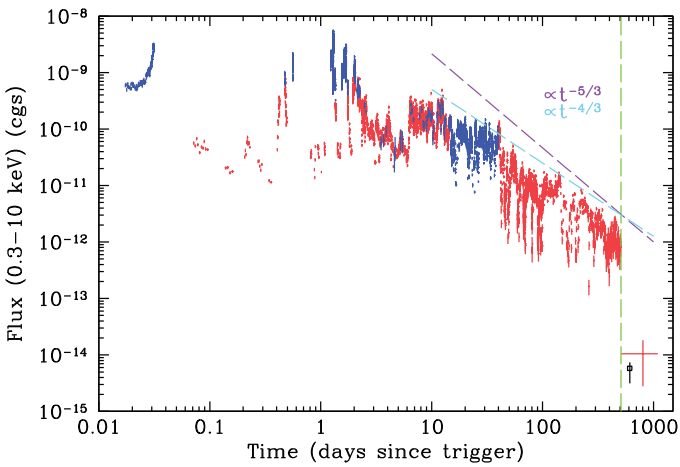

Fig. 6. The long term XRT light curve for Swift J1644+57, the jetted tidal disruption event.[52]

Note that all uncertainties such as beaming angle, accretion efficiency, jet efficiency, etc. cancel out. Using the *Swift*/XRT measured values $f_X, \max \simeq 9 \times 10^{-9}$ erg cm^{-2} s^{-1} and fluence $\Delta E_X \simeq 6 \times 10^{-4}$ erg cm^{-2} yields $t_{\rm fb} + \Delta t_{\rm offset} \simeq 0.9\, d$ for

$\alpha = -5/3$, or $t_{\rm fb} + \Delta t_{\rm offset} \simeq 0.5\,d$ for $\alpha = -4/3$ (Fig. 6, from Ref. 52). These small values $t_{\rm fb} + \Delta t_{\rm offset} \lesssim 1\,d$ argue against the possibility for $\Delta t_{\rm offset} \gtrsim 10\,d$ presented in Tchekhovskoy *et al.*[51]

A value $t_{\rm fb} \lesssim 1\,d$ challenges current theory, which favors $t_{\rm fb} \simeq 20$–$30\ d$, but does not consider strong general relativistic effects in the Kerr metric for large R_T/R_P encounters; modifications in the spread in specific binding energy for the tidal debris from the standard results for $R_T/R_P \simeq 1$ encounters are treated via linear perturbations to a Newtonian gravitational potential (e.g. Refs. 53 and 54 see their Sec. 6).

9. Short versus Long GRBs

Gamma-ray bursts (GRBs) are intense flashes of radiation produced at cosmological distances $z \simeq 2$. GRBs come in two primary flavors, long and short, with the dividing point being roughly 2 s.[55] A further division can be made spectrally according to their hardness ratio (i.e. ratio of high to low energies). The redshift range is from about 0.2 to 2 for *Swift* short GRBs (sGRBs), with a mean of about 0.4. For *Swift* long GRBs (lGRBs) the range is between about 0.009 and 8.2, with a mean of about 2.3 (Fig. 7, from Ref. 56). For sGRBs near enough to be studied in detail, no accompanying supernova is seen. By contrast, nearby lGRBs do have associated supernovae. SGRBs are found in both star-forming and nonstar-forming galaxies; lGRBs are found in star-forming galaxies — typically dwarf irregulars. To date *Swift* has found $\gtrsim$90 sGRBs and $\gtrsim$900 lGRBs.

The typical energy release is $\sim 10^{49}$–10^{50} erg for sGRBs and $\sim 10^{50}$–10^{51} erg for lGRBs. These ranges are based on observed isotropic-equivalent $\sim 10^{53}$ erg for lGRBs, and estimates for jet beaming for each class, $\theta_{\rm j} \sim 5^\circ$ for lGRBs and

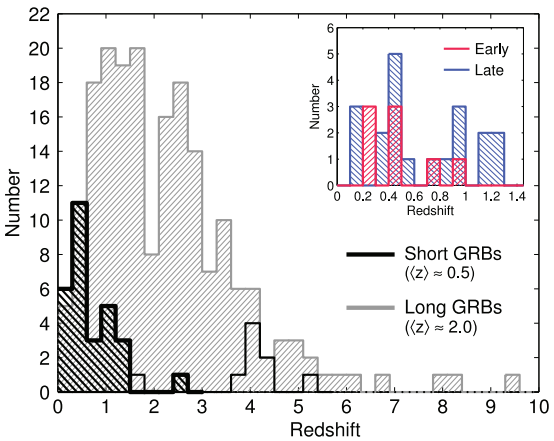

Fig. 7. (Color online) The redshift distribution of sGRBs (black) and lGRBs (gray).[56] Open histogram indicates z upper limits based on the lack of a Lyman-α break in afterglow and/or host galaxy optical detections. Inset shows z distribution of sGRBs by host galaxy type.

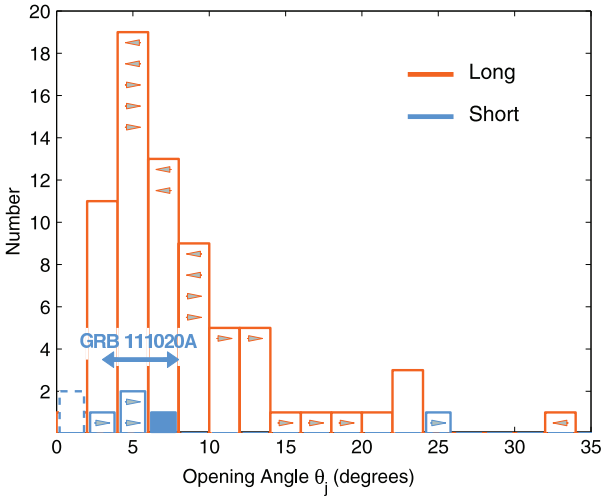

Fig. 8. (Color online) Distribution of opening angles for lGRBs (orange) and sGRBs (blue).[58] Arrows represent upper and lower limits.

$\theta_{\rm j} \sim$5–10° for sGRBs (Burrows *et al.* 2006).[58,59] Beaming angles for sGRBs are still highly uncertain (Fig. 8, from Ref. 58). The $L_{\rm X}/E_{\gamma-{\rm iso}}$ values at 11 hr post-GRB are similar between lGRBs and sGRBs.[59,60] The sGRBs have weaker X-ray afterglows, a mean value of $\sim 7\times10^{-10}$ erg cm^{-2} s^{-1} versus $\sim 3\times10^{-9}$ erg cm^{-2} s^{-1} for lGRBs. Although many of the details are uncertain, the two mechanisms are thought to be collapsars for lGRBs and merging neutron stars for sGRBs.[61] LGRBs are intrinsically very bright, the brightest explosions in the universe. The highest redshift lGRBs were far above detector threshold. SGRBs, by contrast, constitute a flux-limited sample, and are seen primarily nearby, $z \lesssim 1$.

10. Short GRBs: Demographics

Ten years after the discovery of short GRB afterglows more than 90 short GRBs have been found by *Swift* and other γ-ray satellites.[56] A sizable fraction have X-ray and optical afterglows; a few have been detected in the radio. The localizations and optical follow-up work have identified ∼40 host galaxies and enabled detailed studies of the intragalactic locations of short GRBs. An *HST* study of 10 short GRBs within their host galaxies reveals they trace the light distribution of their hosts, while long GRBs are concentrated in the brightest regions of their host galaxies.[62,63]

Fong *et al.*[63] find that the median value of the projected offset from host center for short GRBs of ∼5 kpc is about five times larger than that for the corresponding long GRB median offset. Interestingly, when the two offset distributions are normalized to the size of the host galaxy, they lie almost on top of each other. In other words, the host galaxies for long GRBs are ∼1/5 as large on average than those of

short GRBs. In an updated *HST* study using 22 short GRBs, Fong and Berger[64] refine their previous results, and furthermore find that short GRBs strongly underrepresent their hosts' rest-frame optical and UV light; a fraction ∼0.3–0.45 are located in regions with no stellar light, and ∼0.55 in regions with no UV light. Therefore, Fong and Berger[64] conclude that short GRB progenitors must migrate over considerable distances before their eventual explosions, which supports the idea of progenitor kicks in compact binary systems and the NS–NS merger model for short GRBs.

11. Short GRBs: The Future

What does the future hold for sGRBs? In the next few years as we enter into the detection era for LIGO we will witness opportunities for a LIGO–*Swift* synergism brought about by the detection of NS-BH and NS–NS mergers. By the end of this decade we should have at hand a bonanza of data from gravity wave (GW)/electromagnetic (EM) counterpart detections. It will be rare to catch a jetted afterglow in concert with a GW signal, therefore the great hope is for a "kilonova" associated with the supernovalike transient powered by this radioactive decay of material ejected from the NS during a NS-BH or NS–NS merger. Kilonovae are expected to exhibit a lingering red afterglow (Kasen *et al.* 2013).[66,67]

Observational confirmation of such an event would be important given that this mechanism may be the predominant source of stable $r-$process elements in the universe.[67,68] The biggest problem is that, since the kilonova emission is weak, it could usually be masked by the normal afterglow. GRB 130603B might be the first detected kilonova (Berger, Fong, & Chornock 2013).[71] It was a short GRB at $z = 0.356$ with a duration ∼0.2 s in the BAT. Tanvir *et al.*[69] present optical and near-infrared observations that provide evidence for an accompanying kilonova.

12. Tools to Study the High-z Universe

GRBs are incredibly bright. A typical galaxy at a redshift of only $z = 3$ is fainter than $m \simeq 27$, whereas the optical component of GRB prompt emission, when seen, can be as high as $m \simeq 10$–15. For GRBs, the current record holder is GRB 090429B at $z \simeq 9.4$.[70] Multiwavelength observations of high z GRBs are providing information about the universe at a time when it was only about 4% of its current age, and shed light on the process of reionization in the early universe.[71,72] Strong absorption lines detected in QSO spectra, damped Lyman-α (DLA) systems, originate in galaxies crossing sight lines. A study of the DLA systems associated with optical spectra of GRBs and their hosts has provided detailed information on the metallicity history of the universe, and allowed a comparison of the metallicity history inferred from similar studies involving QSOs. For instance, Savaglio[73] find that the metallicity for GRBs on average is ∼5 times larger than in QSOs (Fig. 9, from Ref. 73).

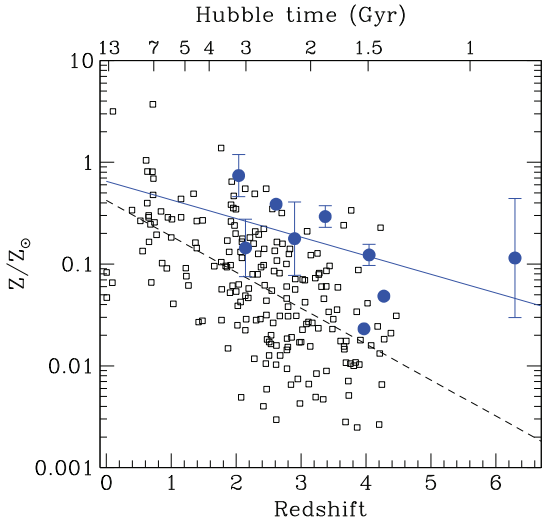

Fig. 9. (Color online) Metallicity redshift evolution measured through DLA absorption for nine GRBs (blue filled circles) and 197 QSOs (open squares).[73] Solid and dashed lines indicate the best-fit linear correlation for GRBs and QSOs, respectively. The metallicity for GRBs on average is ∼5 times larger than in QSOs.

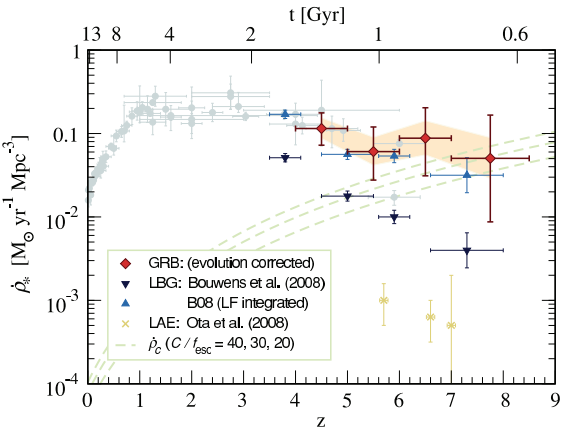

Fig. 10. The cosmic SFR history,[74] with data from several sources.[75–77] The rates inferred from high−z GRBs are shown as diamonds. The three dashed curves[78] give the critical SFR $\dot{\rho}_c$ required to balance recombination, for $C/f_{\rm esc} = 40$, 30 and 20 (top to bottom), where C is the clumpiness of the IGM and $f_{\rm esc}$ the fraction of photons that escape their galaxy.

GRBs are also being used to determine the star formation rate (SFR) to high redshift (Fig. 10, from Ref. 74, 79, 80). Corrections need to be made for systematic effects that alter the proportionality between measured GRB rates and inferred SFRs, such as possible metallicity bias. The SFR from GRBs is higher than from other techniques. GRBs provide a more complete measure of star formation from all types of galaxies.

Table 2. High redshift GRBs.

z	$t_{\rm look\ back}$ (Gyr)	GRB	Brightness		
9.4	13.1	090429B	$K = 19$	@	3 h
8.2	13.0	090423	$K = 20$	@	20 min
$\sim$8	13.0	120923A			
7.5	13.0	100905A	$H \simeq 19$		
6.7	12.8	080813	$K = 19$	@	10 min
6.3	12.8	050904	$J = 18$	@	3 h
6.2	12.8	120521C			
5.6	12.6	060927	$I = 16$	@	2 min
5.3	12.6	050814	$K = 18$	@	23 h
5.11	12.5	060522	$R = 21$	@	1.5 h

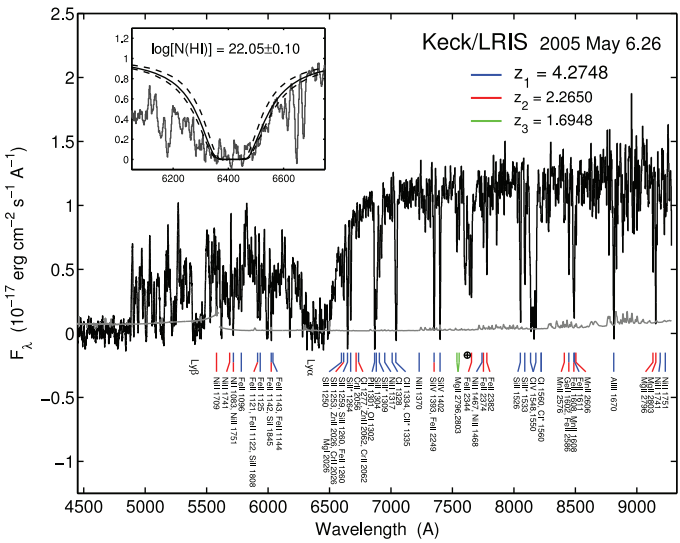

Fig. 11. The optical spectrum of GRB 050505.[86] Lines are seen from the host galaxy at $z = 4.275$ and two foreground absorbers. Inset shows a zoom-in of the Ly-α absorption–solid line shows best fit $\log N({\rm HI}) = 22.05$ and dashed lines indicate ± 1 dex uncertainty.

GRBs, nature's most powerful and luminous explosions, provide us with a means of studying the early universe. GRBs can trace the early time evolution of star formation, reionization, and metallicity. [Lamb & Reichart 2000; Lamb 2002].[81–84] At early times GRBs are a hundred to a thousand times brighter than QSOs; they are also expected to be detected beyond $z \approx 10$, while QSOs diminish rapidly beyond $z \approx 3$. In addition GRB afterglows have simple power-law spectra lacking emission lines, and hence are "clean" probes of the intergalactic medium (IGM). Table 2 gives the ten highest-redshift *Swift* GRBs. About 3% of *Swift* GRBs lie at $z > 5$, lower than pre-*Swift* estimates.[84] Bromm and Loeb[84] also predict that *Swift* can detect GRBs to $z \gtrsim 8$ — three have been seen to date.

Swift's fast localizations are enabling high-z GRB after glow spectroscopy. At low resolution a typical host galaxy appears as a DLA system. In addition, one sees a wealth of metallic lines which can be used to infer metal abundances. At high resolution the host absorption lines split into an array of fine-structure transitions, allowing an inference of gas densities and of conditions associated with diffuse radiation in the host galaxy.[85,86] Figure 11 presents an optical spectrum for GRB 050505 at $z = 4.3$.[86] Numerous lines are apparent, including a DLA feature corresponding to a neutral hydrogen column density of $10^{22}\,\mathrm{cm}^{-2}$. The lines imply a density of $100\,\mathrm{cm}^{-3}$ in the source region. Absorption lines observed in infrared spectroscopic observations of GRB 050904 gave a metallicity measurement of 5% solar,[87] the first metallicity determination at such high redshift, demonstrating that the observed evolution in the mass- and luminosity- metallicity relationships from $z = 0$ to 2 continues to $z > 6$.[86]

13. Conclusion

The sky is rich in transients of many types. *Swift* is exploring the transient sky with unprecedented sensitivity and coverage. Every year brings new discoveries in time domain science. Explosion mechanisms range from gravitational collapse to nuclear burning to B-field reconnection. The future is bright, with new time domain capability across the electromagnetic spectrum, plus wide-field GW, neutrino and cosmic ray detectors coming on board.

References

1. N. Gehrels, G. Chincarini, P. Giommi *et al.*, *Astrophys. J.* **611** (2004) 1005.
2. S. D. Barthelmy, L. M. Barbier, J. R. Cummings *et al.*, *Space Sci. Rev.* **120** (2005) 143.
3. D. N. Burrows, J. E. Hill, J. A. Nousek *et al.*, *Space Sci. Rev.* **120** (2005) 165.
4. P. W. A. Roming, T. E. Kennedy, K. O. Mason *et al.*, *Space Sci. Rev.* **120** (2005) 95.
5. A. V. Gurevich, G. M. Milikh and R. Roussel-Dupré, *Phys. Lett. A* **165** (1992) 463.
6. J. R. Dwyer, *Geophys. Res. Lett.* **30** (2003) 2055.
7. M. S. Briggs, V. Connaughton, C. Wilson-Hodge *et al.*, *Geophys. Res. Lett.* **38** (2011) L02808.
8. E. P. Mazets, S. V. Golentskii, V. N. Ilinskii, R. L. Aptekar and Iu. A. Guryan, *Nature* **282** (1979) 587.
9. C. Thompson and R. C. Duncan, *Mon. Not. R. Astron. Soc.* **275** (1995) 255.
10. R. E. Rothschild, R. E. Lingenfelter, F. D. Seward and O. Vancura, The Compton Gamma Ray Observatory; American Institute of Physics, ed. M. Friedlander, N. Gehrels and R. J. Macomb, Vol. 280 (AIPC, Melville, NY, 1993), p. 808.
11. R. E. Rothschild, S. R. Kulkarni and R. E. Lingenfelter, *Nature* **368** (1994) 432.
12. T. L. Cline, U. D. Desai, G. Pizzichini *et al.*, *Astrophys. J. Lett.* **237** (1980) L1.
13. C. Kouveliotou, T. Strohmayer, K. Hurley *et al.*, *Astrophys. J. Lett.* **510** (1999) L115.
14. C. Thompson and R. C. Duncan, *Astrophys. J.* **561** (2001) 908.

15. R. A. Osten, O. Godet, S. Drake *et al.*, *Astrophys. J.* **721** (2010) 785.
16. R. P. Fender, G. E. Anderson, R. Osten, T. Staley, C. Rumsey, K. Grainge and R. D. E. Saunders, *Mon. Not. R. Astron. Soc.* **446** (2015) L66.
17. J. S. Gallagher and S. Starrfield, *Ann. Rev. Astron. Astrophys.* **16** (1978) 171.
18. G. J. Schwarz, J.-U. Ness, J. P. Osborne *et al.*, *Astrophys. J. Suppl. Ser.* **197** (2011) 31.
19. J. P. Osborne, K. L. Page, A. P. Beardmore *et al.*, *Astrophys. J.* **727** (2011) 124.
20. J. Casares, P. A. Charles and T. Naylor, *Nature* **355** (1992) 614.
21. J. C. A. Miller-Jones, P. G. Jonker, V. Dhawan, W. Brisken, M. P. Rupen, G. Nelemans and E. Gallo, *Astrophys. J. Lett.* **706** (2009) L230.
22. R. Narayan, D. Barret and J. E. McClintock, *Astrophys. J.* **482** (1997) 448.
23. J. K. Cannizzo, W. Chen and M. Livio, *Astrophys. J.* **454** (1995) 880.
24. A. R. King and H. Ritter, *Mon. Not. R. Astron. Soc.* **293** (1998) L42.
25. G. Dubus, J.-M. Hameury and J.-P. Lasota, *Astron. Astrophys.* **373** (2001) 251.
26. B. Warner, *Mon. Not. R. Astron. Soc.* **227** (1987) 23.
27. A. A. Esin, J. E. McClintock and R. Narayan, *Astrophys. J.* **489** (1997) 865.
28. E. Körding, M. Rupen, C. Knigge, R. Fender, V. Dhawan, M. Templeton and T. Muxlow, *Science* **320** (2008) 1318.
29. J. Rodriguez, M. Cadolle Bel, J. Alfonso-Garzón *et al.*, *Astron. Astrophys.* **581** (2015) L9.
30. A. L. King, J. M. Miller, J. Raymond, M. T. Reynolds and W. Morningstar, *Astrophys. J. Lett.* **813** (2015) L37.
31. A. M. Soderberg, E. Berger, K. L. Page *et al.*, *Nature* **453** (2008) 469.
32. P. A. Mazzali, S. Valenti, M. Della Valle *et al.*, *Science* **321** (2008) 1185.
33. J. Frank and M. J. Rees, *Mon. Not. R. Astron. Soc.* **176** (1976) 633.
34. P. J. Young, G. A. Shields and J. C. Wheeler, *Astrophys. J.* **212** (1977) 367.
35. R. Narayan, I. Yi and R. Mahadevan, *Nature* **374** (1995) 623.
36. T. Manmoto, S. Mineshige and M. Kusunose, *Astrophys. J.* **489** (1997) 791.
37. J. Dexter, E. Agol, P. C. Fragile and J. C. McKinney, *Astrophys. J.* **717** (2010) 1092.
38. R. V. Shcherbakov, R. F. Penna and J. C. McKinney, *Astrophys. J.* **755** (2012) 133.
39. F. K. Baganoff, Y. Maeda, M. Morris *et al.*, *Astrophys. J.* **591** (2003) 891.
40. N. Degenaar, J. M. Miller, J. Kennea, N. Gehrels, M. T. Reynolds and R. Wijnands, *Astrophys. J.* **769** (2013) 155.
41. M. J. Rees, *Nature* **333** (1988) 523.
42. E. S. Phinney, in *IAU Symp. 136, The Center of the Galaxy*, ed. M. Morris (Kluwer:Dordrecht, 1989), p. 543.
43. J. K. Cannizzo, H. M. Lee and J. Goodman, *Astrophys. J.* **351** (1990) 38.
44. S. Gezari, D. C. Martin, B. Milliard *et al.*, *Astrophys. J. Lett.* **653** (2006) L25.
45. S. Gezari, S. Basa, D. C. Martin *et al.*, *Astrophys. J.* **676** (2008) 944.
46. S. Komossa, J. Halpern, N. Schartel, G. Hasinger, M. Santos-Lleo and P. Predehl, *Astrophys. J. Lett.* **603** (2004) L17.
47. J. S. Bloom, D. Giannios, B. D. Metzger *et al.*, *Science* **333** (2011) 203.
48. D. N. Burrows, J. A. Kennea, G. Ghisellini *et al.*, *Nature* **476** (2011) 421.
49. A. J. Levan, N. R. Tanvir, S. B. Cenko *et al.*, *Science* **333** (2011) 199.
50. E. Berger, A. Zauderer, G. G. Pooley, A. M. Soderberg, R. Sari, A. Brunthaler and M. F. Bietenholz, *Astrophys. J.* **748** (2012) 36.
51. A. Tchekhovskoy, B. D. Metzger, D. Giannios and L. Z. Kelley, *Mon. Not. R. Astron. Soc.* **437** (2014) 2744.

52. V. Mangano, D. N. Burrows, B. Sbarufatti and J. K. Cannizzo, *Astrophys. J.* **817** (2016) 103.
53. J. Guillochon and E. Ramirez-Ruiz, *Astrophys. J.* **767** (2013) 25.
54. N. Stone, R. Sari and A. Loeb, *Mon. Not. R. Astron. Soc.* **435** (2013) 1809.
55. C. Kouveliotou, C. A. Meegan, G. J. Fishman, N. P. Bhat, M. S. Briggs, T. M. Koshut, W. S. Paciesas and G. N. Pendleton, *Astrophys. J. Lett.* **413** (1993) L101.
56. E. Berger, *Ann. Rev. Astron. Astrophys.* **52** (2014) 43.
57. D. N. Burrows, D. Grupe, M. Capalbi *et al.*, *Astrophys. J.* **653** (2006) 468.
58. W. Fong, E. Berger, R. Margutti *et al.*, *Astrophys. J.* **756** (2012) 189.
59. N. Gehrels, S. D. Barthelmy, D. N. Burrows *et al.*, *Astrophys. J.* **689** (2008) 1161.
60. M. Nysewander, A. S. Fruchter and A. Pe'er, *Astrophys. J.* **701** (2009) 824.
61. N. Gehrels, E. Ramirez-Ruiz and D. B. Fox, *Ann. Rev. Astron. Astrophys.* **47** (2009) 567.
62. E. Berger, S. R. Kulkarni, D. B. Fox *et al.*, *Astrophys. J.* **634** (2005) 501.
63. W. Fong, E. Berger and D. B. Fox, *Astrophys. J.* **708** (2010) 9.
64. W. Fong and E. Berger, *Astrophys. J.* **776** (2013) 18.
65. D. Kasen, N. R. Badnell and J. Barnes, *Astrophys. J.* **774** (2013) 25.
66. D. Grossman, O. Korobkin, S. Rosswog and T. Piran, *Mon. Not. R. Astron. Soc.* **439** (2014) 757.
67. C. Freiburghaus, S. Rosswog and F.-K. Thielemann, *Astrophys. J. Lett.* **525** (1999) L121.
68. S. Goriely, A. Bauswein and H.-T. Janka, *Astrophys. J. Lett.* **738** (2011) L32.
69. N. R. Tanvir, A. J. Levan, A. S. Fruchter, J. Hjorth, R. A. Hounsell, K. Wiersema and R. L. Tunnicliffe, *Nature* **500** (2013) 547.
70. E. Berger, W. Fong and R. Chornock, *Astrophys. J.* **774** (2013) L23.
71. N. R. Tanvir, D. B. Fox, A. J. Levan *et al.*, *Nature* **461** (2009) 1254.
72. R. Salvaterra, M. Della Valle, S. Campana *et al.*, *Nature* **461** (2009) 1258.
73. S. Savaglio, *New J. Phys.* **8** (2006) 195.
74. M. D. Kistler, H. Yüksel, J. F. Beacom, A. M. Hopkins and S. B. Wyithe, *Astrophys. J. Lett.* **705** (2009) L104.
75. A. M. Hopkins and J. F. Beacom, *Astrophys. J.* **651** (2006) 142.
76. R. J. Bouwens, G. D. Illingworth, M. Franx and H. Ford, *Astrophys. J.* **686** (2008) 230.
77. K. Ota, M. Iye, N. Kashikawa *et al.*, *Astrophys. J.* **677** (2008) 12.
78. P. Madau, F. Haardt and M. J. Rees, *Astrophys. J.* **514** (1999) 648.
79. B. E. Robertson and R. S. Ellis, *Astrophys. J.* **744** (2012) 95.
80. M. Trenti, R. Perna and R. Jimenez, *Astrophys. J.* **802** (2015) 103.
81. D. Q. Lamb and D. E. Reichart, *Astrophys. J.* **536** (2000) 1.
82. D. Q. Lamb, *Lighthouses of the Universe*: *The Most Luminous Celestial Objects and Their Use for Cosmology*, Vol. 157 (MPA/ESO, Garching, Germany, 2002).
83. B. Ciardi and A. Loeb, *Astrophys. J.* **540** (2000) 687.
84. V. Bromm and A. Loeb, *Astrophys. J.* **575** (2002) 111.
85. H.-W. Chen, J. X. Prochaska, J. S. Bloom and I. B. Thompson, *Astrophys. J. Lett.* **634** (2005) L25.
86. E. Berger, B. E. Penprase, S. B. Cenko, S. R. Kulkarni, D. B. Fox, C. C. Steidel and N. A. Reddy, *Astrophys. J.* **642** (2006) 979.
87. N. Kawai, G. Kosugi, K. Aoki *et al.*, *Nature* **440** (2006) 184.